文章编号：1001-9014(2024)04-0497-06 DOI:10.11972/j.issn.1001-9014.2024.04.009

Optical facet coatings for high-performance LWIR quantum cascade lasers at λ ~ 8.5 μm

MA Yuan[1,2], LIN Yu-Zhe[1*], WAN Chen-Yang[1,2], WANG Zi-Xian[1,2], ZHOU Xu-Yan[1,3], ZHANG Jin-Chuan[1], LIU Feng-Qi[1], ZHENG Wan-Hua[1,2*]

(1. Laboratory of Solid-State Optoelectronics Information Technology, Institute of Semiconductors, Chinese Academy of Sciences, Beijing 100083, China;
2. Center of Materials Science and Optoelectronics Engineering, University of Chinese Academy of Sciences, Beijing 100049, China;
3. Weifang Academy of Advanced Opto-Electronic Circuits, Weifang 261021, China)

Abstract: We report on the performance improvement of long-wave infrared quantum cascade lasers (LWIR QCLs) by studying and optimizing the anti-reflection (AR) optical facet coating. Compared to the Al_2O_3 AR coating, the Y_2O_3 AR coating exhibits higher catastrophic optical mirror damage (COMD) level, and the optical facet coatings of both material systems have no beam steering effect. A 3-mm-long, 9.5-μm-wide buried-heterostructure (BH) LWIR QCL of λ ~ 8.5 μm with Y_2O_3 metallic high-reflection (HR) and AR of ~ 0.2% reflectivity coating demonstrates a maximum pulsed peak power of 2.19 W at 298 K, which is 149% higher than that of the uncoated device. For continuous-wave (CW) operation, by optimizing the reflectivity of the Y_2O_3 AR coating, the maximum output power reaches 0.73 W, which is 91% higher than that of the uncoated device.

Key words: quantum cascade lasers, long-wave infrared, optical facet coatings, catastrophic optical mirror damage

8.5 μm高性能长波红外量子级联激光器的光学腔面镀膜研究

马　源[1,2]，林羽喆[1*]，万晨杨[1,2]，王紫纤[1,2]，周旭彦[1,3]，张锦川[1]，刘峰奇[1]，郑婉华[1,2*]

(1. 中国科学院半导体研究所 固态光电信息技术重点实验室，北京 100083；
2. 中国科学院大学 材料科学与光电工程中心，北京 100049；
3. 潍坊先进光电芯片研究院，山东 潍坊 261021)

摘要：通过研究和优化长波红外量子级联激光器(LWIR QCLs)的光学腔面增透(AR)膜，可提高器件的输出性能。与Al_2O_3膜系相比，Y_2O_3 AR膜表现出更高的腔面光学灾变(COMD)水平，两种膜系的光学腔面镀膜均无光束转向效应。对激射波长为8.5 μm的3 mm腔长、9.5 μm脊宽掩埋异质结(BH)LWIR QCL使用Y_2O_3膜系的金属高反(HR)膜和反射率约0.2%的AR膜，在298 K下获得了2.19 W的最高脉冲峰值功率，较未镀膜器件提高149%。对于连续波(CW)操作，通过优化Y_2O_3 AR膜的反射率，最高输出功率达到0.73 W，较未镀膜器件提高91%。

关　键　词：量子级联激光器；长波红外；光学腔面镀膜；腔面光学灾变

中图分类号：O43；TN248.4　　**文献标识码**：A

Introduction

As a significant candidate for highly efficient and compact mid-infrared (MIR) to terahertz light sources, quantum cascade lasers (QCLs) have shown tremendous potential in applications such as chemical and biological sensing[1-2], free space optical communication[3], and infrared countermeasures (IRCM)[4]. Among them, more

Received date: 2023-11-22, **revised date**: 2023-12-15　**收稿日期**：2023-11-22，**修回日期**：2023-12-15
Foundation items: Supported by the National Natural Science Foundation of China (12393830)
Biography: MA Yuan (1997-), male, Xincai, Henan, Ph. D. Research area involves semiconductor materials and devices. E-mail: mayuan@semi.ac.cn
* **Corresponding authors**: E-mail: linyuzhe@semi.ac.cn, whzheng@semi.ac.cn

and more attentions have been devoted to the development of long-wave infrared (LWIR, $\lambda \approx$ 8-12 μm) QCLs with high output power, high wall-plug efficiency (*WPE*) and good beam quality[5-7]. However, some problems still need to be solved, which brings greater challenges to the performance improvement of LWIR QCLs. First, additional waveguide designs or thicker epitaxial structures need to be considered in order to maintain optical confinement factor of LWIR QCLs[8]. Otherwise, the reduction in mode gain, the increase in free carrier absorption losses (proportional to λ^2) and the enhancement of plasmonic mode coupling at the metal-semiconductor interface will significantly deteriorate the device performance[9]. Second, optical facet coating, as a key technology, has important applications in power extraction[10], self-lasing suppression of single-mode lasers[11], etc. Nevertheless, the cavity facet coating of LWIR QCLs requires not only increasing thickness of anti-reflection (AR) coating to match the target wavelength[12], but also selecting an appropriate coating material to reduce the facet optical absorption, thereby improving the level of catastrophic optical mirror damage (COMD)[13]. Additionally, it is necessary to avoid deterioration of beam quality due to the beam steering effect[14]. Metallic high-reflection (HR) coatings have been commonly used and studied in LWIR QCLs to improve one facet output power[15-17]. Currently, there are relatively few reports on the optimization of AR coatings.

In this letter, two types of optical facet coatings (Al_2O_3 and Y_2O_3) were demonstrated and compared on 8.5 μm LWIR QCLs for the selection of appropriate coating material. By optimizing a single-layer Y_2O_3 AR coating on the 3-mm-long buried-heterostructure (BH) LWIR QCLs, the continuous-wave (CW) and pulsed performance have been significantly improved. Corresponding deterioration of far-field characteristics after coating was not observed.

1 Wafer structure, fabrication and testing

The LWIR QCL wafer, lasing wavelength close to 8.5 μm, is based on a single phonon resonance-continuum depopulation structure with 35 cascade stages. The active region consists of lattice-matched $In_{0.53}Ga_{0.47}As$/$In_{0.52}Al_{0.48}As$ layers as previously shown in Ref. [18]. The double channel ridge structure with an average ridge width of 9.5 μm was first fabricated by contact photolithography and wet chemical etching. Then, semi-insulating InP:Fe was grown by MOCVD in order to confine the carriers and reduce the sidewall optical losses. A 400-nm-thick SiO_2 layer was deposited by Plasma Enhanced Chemical Vapor Deposition (PECVD) for insulation, and a Ti/Au top contact layer was deposited by e-beam evaporation for electrical contacts. An additional 5-μm-thick gold layer was subsequently electroplated to further improve the heat dissipation. After thinned to 120 μm, an AuGeNi/Au bottom contact layer was deposited on the substrate. The processed QCL wafer was cleaved into bars with a cavity length of 3 mm for facet coating.

The uncoated and coated devices were mounted epi-side down on diamond submounts with indium for higher heat dissipation efficiency. The CW and pulsed (5 kHz, 1 μs) performance were characterized by a Thorlabs S450C calibrated thermopile power meter and an IS50R Fourier Transform Infrared (FTIR) spectrometer. We used the rotation method to test the far-field divergence angle and built an automated scanning system.

2 Coating material processing and comparison

Dielectric material used as LWIR QCLs facet coating must have low absorption in the LWIR range and mature fabrication process to ensure that the AR coating does not suffer from COMD. For this purpose, Al_2O_3 and Y_2O_3 facet coating material systems were studied from the same wafer with 3 mm cavity length. The metallic HR coating consisting of M_2O_3/Ti/Au/M_2O_3 was coated on the back facet, as shown in Fig. 1(a). The AR coating was the single-layer of M_2O_3 coated on the front facet, where M_2O_3 represented Al_2O_3 or Y_2O_3. A dielectric material M_2O_3 was deposited on the back facet using e-beam evaporation to provide electrical insulation from Au. After that, a thin layer of Ti was sputtered to increase the adhesion between M_2O_3 and Au. Next, 100 nm of Au with a high refractive index was used to achieve a high reflection of nearly 100% for the LWIR QCLs. Finally, another layer of dielectric material M_2O_3 was deposited to complete the HR coating to avoid short-circuiting of the devices in the subsequent packaging process. E-beam evaporation was chosen to deposit a single-layer of M_2O_3 AR coating. The AR reflectivity between 27% (uncoated) and close to 0% (quarter-wave layer) can be adjusted by simply adjusting the coating thickness[10]. The AR and HR scanning electron microscope (SEM) images of Y_2O_3 material system are shown in Figs. 1(b) and 1(c).

Simulation based on characteristic transfer matrix

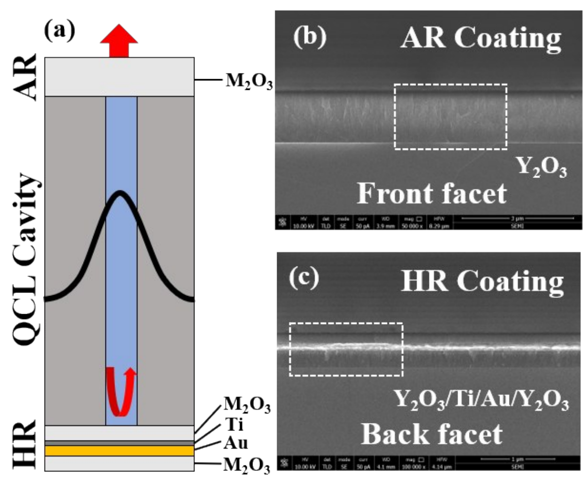

Fig. 1 Schematic diagram of the LWIR QCLs: (a) schematic diagram of the LWIR QCLs with AR and HR coatings applied to the front and back facets; scanning electron microscopy (SEM) images of coatings on (b) front and (c) back facet

图1 LWIR QCLs示意图:(a)LWIR QCLs前、后腔面AR和HR膜的示意图;(b)前和(c)后腔面膜的扫描电镜图

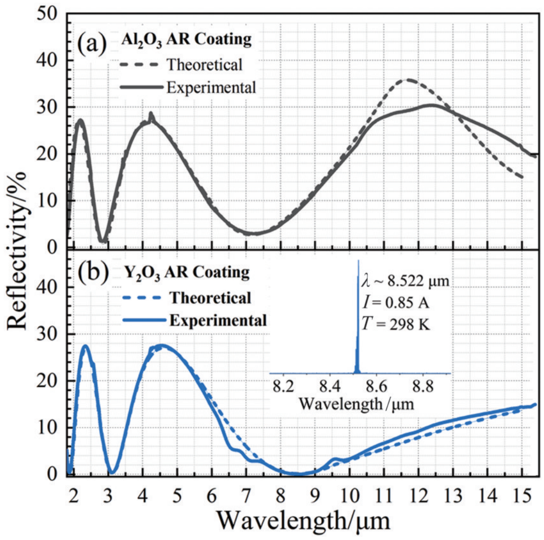

Fig. 2　Reflectivity curves: experimental and theoretically simulated reflectivity curves of (a) Al_2O_3 and (b) Y_2O_3 AR coatings, the inset shows the lasing spectrum of the LWIR QCL at 298 K
图2　反射率曲线：(a)Al_2O_3和(b)Y_2O_3 AR膜的实验和理论模拟反射率曲线，插图是LWIR QCL在298 K的激射光谱

was derived to determine the coating thickness at the corresponding reflectivity. Reflectivity measurements were performed on an FTIR spectrometer with an MCT detector. Figure 2 shows the optical curves of the simulations and measurements of the Al_2O_3 and Y_2O_3 AR coatings. The wavelength for an uncoated LWIR QCL is shown in the inset. The theoretical simulations are in good agreement with the experimental measurements.

For the Al_2O_3 material system, the thickness at quarter-wave layer exceeds 2 μm, which poses great difficulties in manufacturing. Therefore, in the initial stage, we selected a single-layer Al_2O_3 AR coating with a reflectivity of ~ 8.0% by reducing the thickness, and the HR coating was Al_2O_3/Ti/Au/Al_2O_3. The CW light-current-voltage (*L*–*I*–*V*) and *WPE* curves of uncoated and HR-AR (*R*≈8%) coated devices operating at 298 K are shown in Fig. 3(a). Among them, the solid lines in the black and red circles represent the voltage and optical power curves, respectively, while the dashed lines in the blue circle represent the *WPE* curve. Compared with uncoated and coated devices, the slope efficiency (η_s) has been improved from 0.42 W/A to 0.7 W/A, while *WPE* has been increased from 1.6% to 2.7%. Moreover, the maximum output power (P_{max}) increased from 0.25 W to 0.33 W. However, the coated devices using Al_2O_3 exhibit COMD at the power density level of ~ 1.73 MW/cm²

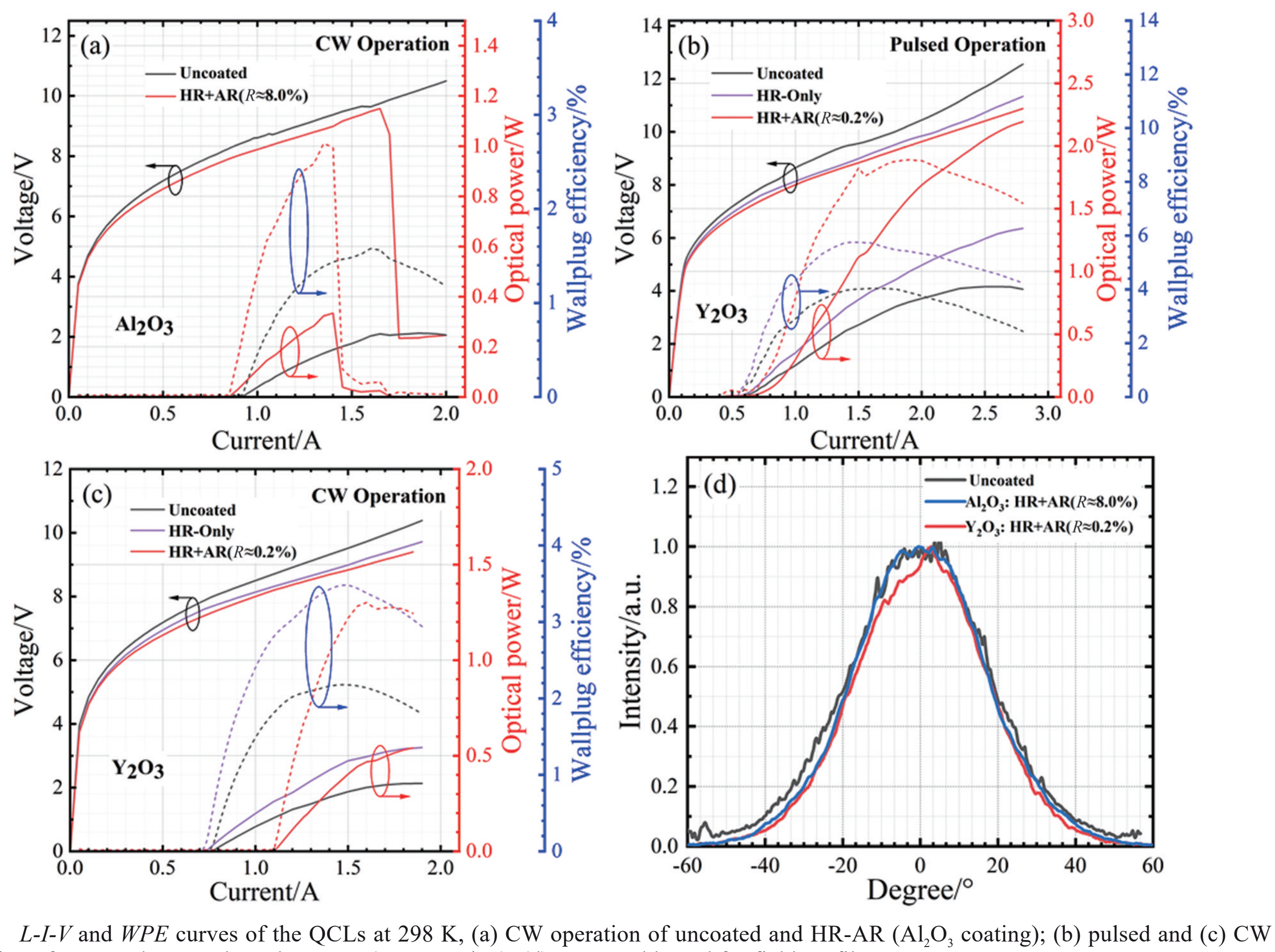

Fig. 3　*L-I-V* and *WPE* curves of the QCLs at 298 K, (a) CW operation of uncoated and HR-AR (Al_2O_3 coating); (b) pulsed and (c) CW operation of uncoated, HR-only and HR-AR (Y_2O_3 coating); (d) measured lateral far-field profiles
图3　QCL在298 K时的*L-I-V*和WPE曲线，(a)连续操作的未镀膜、AR-HR(Al_2O_3膜系)器件；(b)脉冲和(c)连续操作的未镀膜、仅HR和AR-HR(Y_2O_3膜系)器件；(d)测量的水平远场分布

before thermal inversion, as shown in Fig. 4(a). This also shows that Al_2O_3 coating has high absorption in the LWIR range[19], with an absorption coefficient as high as 755.2 cm^{-1} at 8.5 μm, which is not suitable for power extraction of high-performance LWIR QCLs.

In comparison, the Y_2O_3 material system exhibits better performance. Since Y_2O_3 has a higher refractive index in the LWIR range, the thickness of the AR coating is initially set to quarter-wave layer with reflectivity of ~0.2%. The pulsed *L-I-V* and *WPE* curves of uncoated, HR-only and HR-AR coated devices operating at 298 K are shown in Fig. 3(b). η_s is from 0.65 W/A for uncoated, 0.88 W/A for HR-only, to a higher value of 1.63 W/A for HR-AR device. *WPE* is from 4.0%, 5.8% to 8.8% and P_{max} from 0.88 W, 1.34 W to 2.19 W. The HR-AR coated device shows 120% and 149% improvements in *WPE* and P_{max}, respectively, compared to uncoated device under 298 K in pulsed mode. Since the absorption coefficient of Y_2O_3 at 8.5 μm is only 8.3 cm^{-1}[20-21]. The cavity facet remained normally after the test, as shown in Fig. 4(b). The COMD has not occurred until the power density reached 11.5 MW/cm^2. The *L-I-V* and *WPE* curves of these devices under 298 K CW operation are shown in Fig. 3(c), representing an improvement of η_s from 0.50 W/A for uncoated, 0.68 W/A for HR-only, to 1.07 W/A for HR-AR laser, *WPE* from 2.2%, 3.5% to 3.3% and P_{max} from 0.35 W, 0.54 W to 0.54 W.

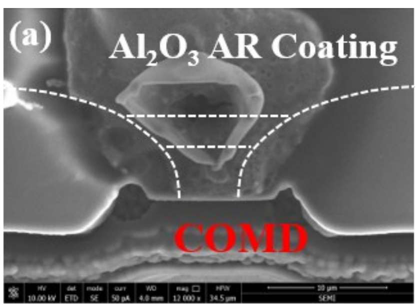

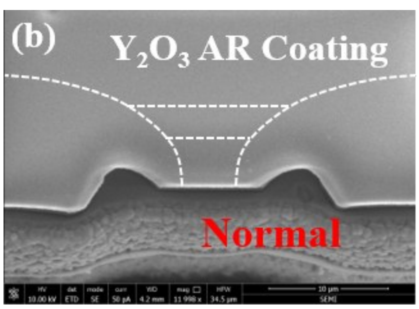

Fig. 4 SEM image of the front facet of the laser coated with (a) Al_2O_3 and (b) Y_2O_3 AR coating after testing
图4 镀(a)Al_2O_3和(b)Y_2O_3 AR膜的激光器在测试后的前腔面扫描电镜图

Under CW operation, the *WPE* and P_{max} of the HR-AR coated device increased by 50% and 54% respectively, compared to that of the uncoated device. However, it showed no significant improvement compared to the only-HR device. The threshold current density J_{th} of LWIR QCLs is defined as[22]:

$$J_{th} = J_{tr} + \frac{\alpha_w + \alpha_m}{g\Gamma} \quad , \quad (1)$$

where J_{tr} is the transparency current, α_w is the internal loss of the laser waveguide, $\alpha_m = (1/2L)ln[1/R_{front}R_{back}]$ is the overall mirror loss, L is the length of the cavity, and $g\Gamma$ is the differential modal gain. α_m increases significantly from 2.2 cm^{-1} for the only-HR device to 10.4 cm^{-1} for the HR-AR ($R\approx0.2\%$) device. According to Eq. (1), the J_{th} of CW operation significantly increases from 2.50 kA/cm^2 to 3.82 kA/cm^2. This substantial increase in the threshold current density brings additional self-heating effects to the devices[15], which appears to impede the AR coating from extracting further power.

One concern with optical coatings is the beam steering effect[12, 14]. Conversely, the lateral far-field divergence angle of the HR+AR devices with Al_2O_3 and Y_2O_3 coatings shown in Fig. 3(d) is consistent with that of the uncoated device and shows no shift or beam steering effect. This can be explained as the negligible thickness of the coating compared to the length of the cavity.

3 Coating design and results

Despite the AR coating with near 0% reflectivity achieved significant improvements in output performance under pulsed operation. Nevertheless, for LWIR QCLs, it is necessary to optimize the reflectivity for ensuring further improvement of P_{max} and *WPE* under CW operation. The slope efficiency η_s of LWIR QCLs is defined as[23]:

$$\eta_s = \frac{N}{1 + 1/\beta}\eta_i\left(\frac{\alpha_m}{\alpha_m + \alpha_w}\right), \quad \beta = \frac{1 - R_{front}}{1 - R_{back}}\sqrt{\frac{R_{back}}{R_{front}}} \quad , \quad (2)$$

where β takes into account the unequal power distribution from asymmetry in facet reflectivity[24], N is the number of stages, and η_i is the internal quantum efficiency per stage. R_{back} and R_{front} are the reflectivity of the back and front facets. According to Eqs. (1) and (2), we can derive the internal parameters of the laser through the changes in J_{th} and η_s of devices with different coating states (different α_m) under pulsed operation, as follows: J_{tr}=1.43 kA/cm^2, α_w=2.1 cm^{-1}, $g\Gamma$=8.8 cm/kA[10]. By introducing the additional resonant waveguide loss $\alpha_{w,res}$=$g\Gamma J_{tr}$=12.6 cm^{-1}, the total waveguide loss is obtained as $\alpha_w+\alpha_{w,res}$=14.7 cm^{-1}[25].

In the simple Rigrod analysis, i.e. [26], assuming uniform gain saturation, the device WPE η_W at the roll-over current density J_{max} can be expressed as[10]:

$$\eta_W = \frac{Nh\nu}{eV_{max}}\left(1 - \frac{J_{th}}{J_{max}}\right)\eta_i\frac{\alpha_m}{\alpha_w + \alpha_m} \quad , \quad (3)$$

where $h\nu$ is the photon energy, V_{max} is the voltage at J_{max}. Therefore, for LWIR QCLs, the back cavity is generally a metallic HR coating, and the appropriate R_{front} is selected by adjusting the front cavity AR coating to achieve both high η_s and *WPE*. Figure 5 shows the *WPE* and AR

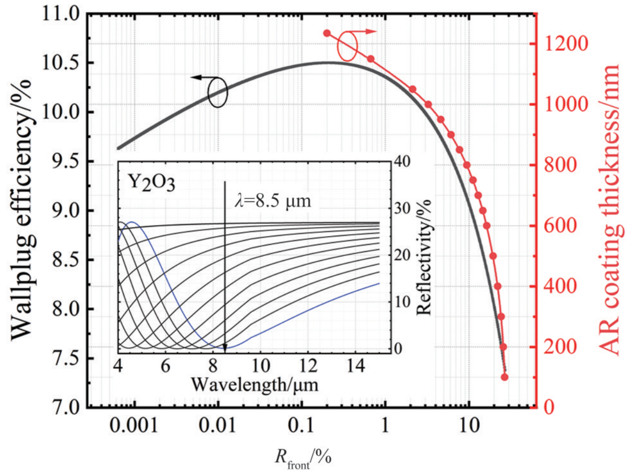

Fig. 5 Predicted *WPE* and AR coating thickness as a function of front facet AR reflectivity, inset: the reflectivity curves for different Y_2O_3 AR coating thicknesses

图 5 预测的 WPE 和 AR 膜厚度与前腔面 AR 膜反射率函数关系,插图:不同 Y_2O_3 AR 膜厚度的反射率曲线

coating thickness as a function of R_{front} predicted by Eq. (3) using the above internal parameter. The inset shows the reflectivity curves for different Y_2O_3 AR coating thicknesses, where R_{front} increases from 0.2% to 27% by reducing the coating thickness, starting from a quarter-wave thickness. The measured *WPE* is approximately 18% lower than the model predictions due to the reduced slope efficiency between the threshold and the roll-over[10]. Although the pulsed *WPE* is maximum at R_{front}= 0.2% coincidentally and then decreases with increasing front cavity reflectivity, R_{front}=0.2% is not conducive to power extraction for the CW operation. Therefore, in order to ensure a high *WPE* and prevent the additional self-heating effect caused by the increase in J_{th}, the 3-mm-long device was chosen with the same α_m=4.4 cm^{-1} as the uncoated device. Finally, an 850 nm single-layer Y_2O_3 AR coating with a reflectivity of about 7.5% was applied by adjusting the AR coating thickness.

The *L-I-V* and *WPE* curves of the HR-AR (R≈7.5%) coated device under 298 K pulsed and CW operation are shown in Figs. 6 (a) and 6(b) respectively. The threshold current density under pulsed operation is J_{th}=1.79 kA/cm^2, along with η_s= 1.15 W/A, *WPE*= 7.20% and P_{max}=1.65 W, and the threshold current density under CW operation is J_{th}=2.71 kA/cm^2, along with η_s= 0.93 W/A, *WPE*=4.18% and P_{max}=0.73 W. After the optimization of AR coating reflectivity, compared to the uncoated device, the HR-AR device showed 80% and 88% improvements in *WPE* and P_{max} under pulsed operation, respectively, while significant improvements of 106% and 91% were also obtained under CW operation. A more suitable reflectivity may exist at R_{front}=0.2% to 7.5%, allowing the power extraction under CW operation to be further increased. Furthermore, utilizing a device of the same size as in Ref. [18] along with Y_2O_3 coatings with optimized reflectivity, the output performance will be significantly improved.

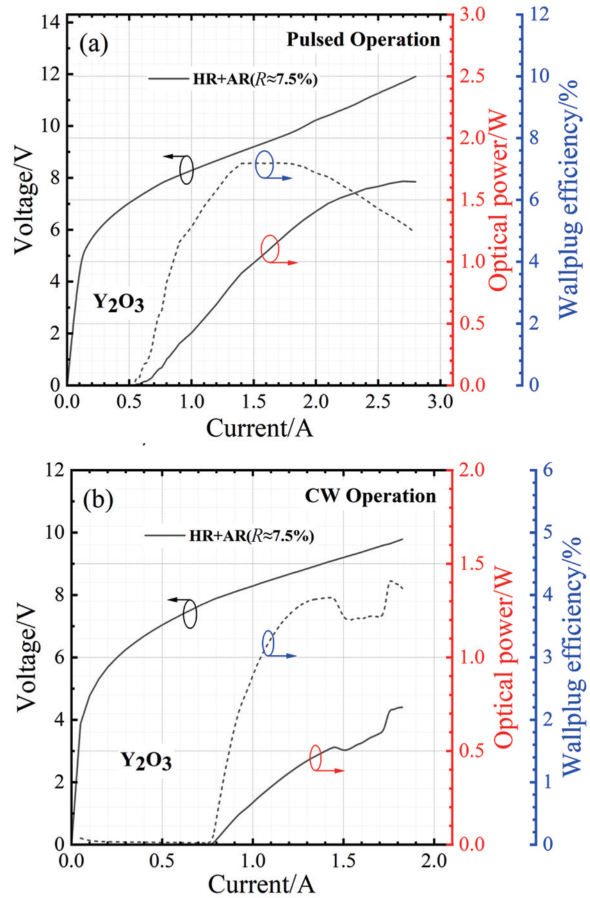

Fig. 6 *L-I-V* and *WPE* curves of the QCL with optimized front facet Y_2O_3 AR coating reflectivity under (a) pulsed and (b) CW operation at 298 K

图 6 具有优化前腔面 Y_2O_3 AR 膜反射率的 LWIR QCL 在 298 K 时(a)脉冲和(b)连续操作下的 *L-I-V* 和 WPE 曲线

4 Conclusions

In summary, we compared the application of Al_2O_3 and Y_2O_3 coatings in LWIR QCLs without beam steering effect, and proved that Y_2O_3 was more suitable for power extraction of high-performance LWIR QCLs compared to Al_2O_3. The LWIR QCL with λ~8.5 μm was applied with a Y_2O_3 coating with a reflectivity close to 0%, which was suitable for power extraction under pulsed operation and obtained a peak power of 2.19 W and *WPE* of 8.8%. Considering self-heating effects, the Y_2O_3 AR coated device with a reflectivity of 7.5% showed a maximum pulsed peak power of 1.65 W and CW output power of 0.73 W at 298 K, which were 88% and 91% higher than uncoated lasers, respectively. In the future, by improving the epitaxial performance and combining the power extraction of Y_2O_3 AR coating, higher performance LWIR QCLs will be obtained.

References

[1] Sharma R C, Kumar S, Kumar S, *et al*. Photoacoustic remote sensing of suspicious objects for defence and forensic applications [J]. *Spectrochimica Acta Part A: Molecular and Biomolecular Spectroscopy*, 2020, **224**: 117445.

[2] SUN Y Q, YANG K, LIU J H, *et al*. High sensitivity and fast detec-

tion system for sensing of explosives and hazardous materials [J]. *Sensors and Actuators B-Chemical*, 2022, **360**: 131640.

[3] Spitz O, Didier P, Durupt L, *et al*. Free-space communication with directly modulated mid-Infrared quantum cascade devices [J]. *IEEE Journal of Selected Topics in Quantum Electronics*, 2022, **28**(1): 1-9.

[4] Patel C K N, Lyakh A, Maulini R, *et al*. QCL as a game changer in MWIR and LWIR military and homeland security applications [C]. Micro-and Nanotechnology Sensors, Systems, and Applications IV. SPIE, 2012, **8373**: 599-607.

[5] ZHOU W, LU Q Y, WU D H, *et al*. High-power, continuous-wave, phase-locked quantum cascade laser arrays emitting at 8 μm [J]. *Opt Express*, 2019, **27**(11): 15776-15785.

[6] Schundler E C, Mansur D J, Hilton M, *et al*. Multipath extinction detector for chemical sensing [C]. Chemical, Biological, Radiological, Nuclear, and Explosives (CBRNE) Sensing XXIII. SPIE, 2022, **12116**: 208-217.

[7] Joharifar M, Dely H, PANG X D, *et al*. High-speed 9.6-μm long-wave infrared free-space transmission with a directly-modulated QCL and a fully-passive QCD [J]. *Journal of Lightwave Technology*, 2023, **41**(4): 1087-1094.

[8] Troccoli M, Lyakh A, FAN J Y, *et al*. Long-wave IR quantum cascade lasers for emission in the λ=8-12 μm spectral region [J]. *Optical Materials Express*, 2013, 3(9): 1546-1560.

[9] XIE F, Caneau C, Leblanc H P, *et al*. Watt-level room temperature continuous-wave operation of quantum cascade lasers with λ>10 μm [J]. *IEEE Journal of Selected Topics in Quantum Electronics*, 2013, **19**(4): 1200407.

[10] Maulini R, Lyakh A, Tsekoun A, *et al*. High power thermoelectrically cooled and uncooled quantum cascade lasers with optimized reflectivity facet coatings [J]. *Applied Physics Letters*, 2009, **95**(15): 151112.

[11] ZHOU W J, WU D H, LU Q Y, *et al*. Single-mode, high-power, mid-infrared, quantum cascade laser phased arrays [J]. *Scientific Reports*, 2018, **8**: 14866.

[12] Nguyen J, YU J S, Evans A, *et al*. Optical coatings by ion-beam sputtering deposition for long-wave infrared quantum cascade lasers [J]. *Applied Physics Letters*, 2006, **89**(11): 111113.

[13] WANG F H, Slivken S, Razeghi M. High-brightness LWIR quantum cascade lasers [J]. *Optics Letters*, 2021, **46**(20): 5193-5196.

[14] Herzog W D, Goldberg B B, Ünlü M S. Beam steering in narrow-stripe high-power 980-nm laser diodes [J]. *IEEE Photonics Technology Letters*, 2000, **12**(12): 1604-1606.

[15] Page H, Collot P, Rossi A D, *et al*. High reflectivity metallic mirror coatings for mid-infrared (λ≈9 μm) unipolar semiconductor lasers [J]. *Semiconductor Science and Technology*, 2002, **17**(12): 1312.

[16] NIU S Z, LIU J Q, ZHAO Y, *et al*. High-performance bound-to-continuum quantum cascade lasers at λ~8 μm [J]. *Journal of Nanoscience and Nanotechnology*, 2018, **18**(11): 7498-7501.

[17] SUN Y Q, YIN R, ZHANG J C, *et al*. High-performance quantum cascade lasers at λ~9 μm grown by MOCVD [J]. *Optics Express*, 2022, **30**(21): 37272-37280.

[18] FEI T, ZHAI S, ZHANG J, *et al*. High power λ~8.5 μm quantum cascade laser grown by MOCVD operating continuous-wave up to 408 K [J]. *Journal of Semiconductors*, 2021, **42**(11): 112301.

[19] Kischkat J, Peters S, Gruska B, *et al*. Mid-infrared optical properties of thin films of aluminum oxide, titanium dioxide, silicon dioxide, aluminum nitride, and silicon nitride [J]. *Applied Optics*, 2012, **51**(28): 6789-6798.

[20] Nigara Y. Measurement of the optical constants of yttrium oxide [J]. *Japanese Journal of Applied Physics*, 1968, **7**(4): 404.

[21] Tropf W J, Thomas M E. Yttrium oxide (Y_2O_3) [M]. Handbook of Optical Constants of Solids. Academic Press, 1997: 1079-1096.

[22] Slivken S, Evans A, YU J S, *et al*. High power, continuous-wave, quantum cascade lasers for MWIR and LWIR applications [C]. Quantum Sensing and Nanophotonic Devices III. SPIE, 2006, **6127**: 15-24.

[23] YU J S, Slivken S, Evans A J, *et al*. High-performance continuous-wave operation of λ~4.6 μm quantum-cascade lasers above room temperature [J]. *IEEE Journal of Quantum Electronics*, 2008, **44**(8): 747-754.

[24] Vanderziel J P, Logan R A, Dupuis R D. High-power (AlGa)As strip-buried heterostructure lasers [J]. *IEEE Journal of Quantum Electronics*, 1985, **21**(10): 1659-1665.

[25] Wittmann A, Hugi A, Gini E, *et al*. Heterogeneous high-performance quantum-cascade laser sources for broad-band tuning [J]. *IEEE Journal of Quantum Electronics*, 2008, **44**(11): 1083-1088.

[26] Rigrod W W. Homogeneously broadened CW lasers with uniform distributed loss [J]. *IEEE Journal of Quantum Electronics*, 1978, **14**(5): 377-381.